JACS
JOURNAL OF THE AMERICAN CHEMICAL SOCIETY

ARTICLE

pubs.acs.org/JACS

Hydrogen Bonding and Spin Density Distribution in the Q_B Semiquinone of Bacterial Reaction Centers and Comparison with the Q_A Site

Erik Martin,[†] Rimma I. Samoilova,[⊥] Kupala V. Narasimhulu,[‡] Tzu-Jen Lin,[¶] Patrick J. O'Malley,[*,¶] Colin A. Wraight,[*,†,§] and Sergei A. Dikanov[*,‡]

[†]Center for Biophysics & Computational Biology, [‡]Department of Veterinary Clinical Medicine, and [§]Department of Biochemistry, University of Illinois at Urbana−Champaign, Urbana, Illinois 61801, United States

[⊥]Institute of Chemical Kinetics and Combustion, Russian Academy of Sciences, Novosibirsk 630090, Russia

[¶]School of Chemistry, University of Manchester, Manchester M13 9PL, U.K.

Supporting Information

ABSTRACT: In the photosynthetic reaction center from *Rhodobacter sphaeroides*, the primary (Q_A) and secondary (Q_B) electron acceptors are both ubiquinone-10, but with very different properties and functions. To investigate the protein environment that imparts these functional differences, we have applied X-band HYSCORE, a 2D pulsed EPR technique, to characterize the exchangeable protons around the semiquinone (SQ) in the Q_A and Q_B sites, using samples of ^{15}N-labeled reaction centers, with the native high spin Fe^{2+} exchanged for diamagnetic Zn^{2+}, prepared in ^1H_2O and ^2H_2O solvent. The powder HYSCORE method is first validated against the orientation-selected Q-band ENDOR study of the Q_A SQ by Flores et al. (*Biophys. J.* **2007**, *92*, 671−682), with good agreement for two exchangeable protons with anisotropic hyperfine tensor components, T, both in the range 4.6−5.4 MHz. HYSCORE was then applied to the Q_B SQ where we found proton lines corresponding to $T \approx 5.2$, 3.7 MHz and $T \approx 1.9$ MHz. Density functional-based quantum mechanics/molecular mechanics (QM/MM) calculations, employing a model of the Q_B site, were used to assign the observed couplings to specific hydrogen bonding interactions with the Q_B SQ. These calculations allow us to assign the $T = 5.2$ MHz proton to the His-L190 $N_\delta H\cdots O_4$ (carbonyl) hydrogen bonding interaction. The $T = 3.7$ MHz spectral feature most likely results from hydrogen bonding interactions of O1 (carbonyl) with both Gly-L225 peptide NH and Ser-L223 hydroxyl OH, which possess calculated couplings very close to this value. The smaller 1.9 MHz coupling is assigned to a weakly bound peptide NH proton of Ile-L224. The calculations performed with this structural model of the Q_B site show less asymmetric distribution of unpaired spin density over the SQ than seen for the Q_A site, consistent with available experimental data for ^{13}C and ^{17}O carbonyl hyperfine couplings. The implications of these interactions for Q_B function and comparisons with the Q_A site are discussed.

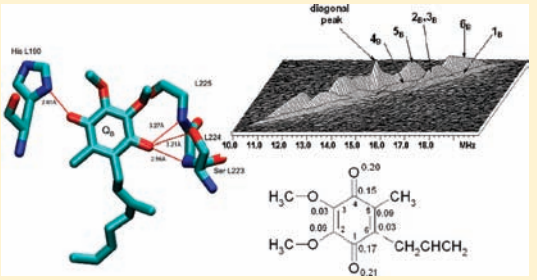

INTRODUCTION

The primary event in photosynthesis is light-driven charge separation, catalyzed by the reaction center (RC), a (bacterio) chlorophyll-containing protein complex. Light activation results in electron transfer from the primary donor, P, a dimer of (bacterio) chlorophyll, through a series of cofactors of low potential. On time scales longer than a nanosecond, the charge separation in RCs from purple bacteria resides on the primary donor and on the acceptor quinones. The primary quinone, Q_A, is tightly bound and functions as a one-electron redox species, whereas the secondary quinone, Q_B, is reversibly bound and can be doubly reduced via Q_A^-, with the uptake of two protons (reviewed in refs 1−3). Despite these marked functional differences, in *Rba. sphaeroides* the two quinones are chemically identical ubiquinone-10 molecules,[1−4] presenting an ideal opportunity to study the effect of protein structure on cofactor redox properties. The two neutral forms of Q_B, quinone and quinol, are rapidly exchangeable, but the semiquinone (SQ) intermediate, Q_B^-, is tightly bound and stabilized, contributing to the redox properties of both reduction steps. It can be expected that hydrogen-bonding underlies this stability.

From the known structures of bacterial RCs, Q_A and Q_B are positioned symmetrically about an iron-histidine, Fe^{2+}-$(His)_4$, complex, and both quinones are bound by hydrogen bonds to the protein (Figure 1).[5,7,8] However, the plethora of X-ray structures now available does not provide unequivocal descriptions of the two quinone sites. The C_4 carbonyl of Q_A is hydrogen-bonded to N_δ of His-M219 (an Fe-ligand), while the backbone NH of Ala-M260 is a H-bond donor to the C_1 carbonyl.[7] On the other hand,

Received: January 7, 2011
Published: March 18, 2011

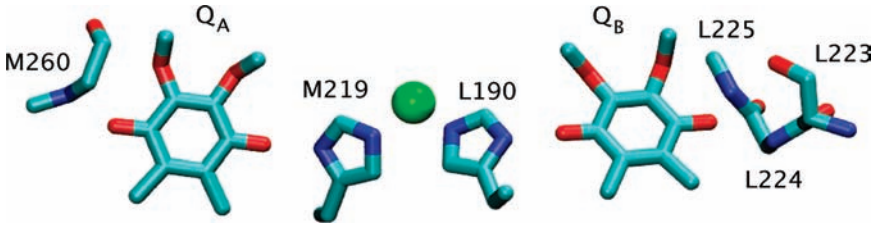

Figure 1. Essential features of the Q_A and Q_B binding sites, showing putative hydrogen-bond donors to the quinone carbonyls. The structure is from PDB i.d. 1dv3.[8] The figure was prepared in VMD.[42]

the H-bond distances and the torsional angles of the two methoxy group substituents of the ubiquinone ring are quite variable in different structures (reviewed in ref 3).

For the Q_B site, crystal structures show even more diversity, including at least two different positions relative to the Fe^{2+}-$(His)_4$ complex.[7−9] The functional position has been established to be the proximal location, essentially symmetrical to the position of Q_A. In the proximal position, Q_B is clearly hydrogen-bonded through the C_4 carbonyl to N_δ of His-L190 (an Fe-ligand), but a second H-bond to the C_1 carbonyl is variously indicated from the backbone NH groups of Ile-L224 and/or Gly-L225 as potential donors (Figure 1).[7−9] The hydroxyl from Ser-L223 is also thought to form a hydrogen bond with either the quinone C_1 carbonyl, especially in the semiquinone state, or Asp-L213.[2,3,6,10] An additional H-bond from the peptide NH of Thr-L226 to one methoxy group was inferred from a recent structure.[9] Thus, in addition to uncertainties in the geometry of the H-bonds to Q_B, even the number is uncertain.

Equivalent knowledge of the oxidized and reduced (SQ) states is necessary to understand the chemical reactivities and kinetic pathways of Q_A^- and Q_B^-, but the H-bond environment around the semiquinone states is not indicated by the crystal structures. This, however, can be addressed through the application of pulsed EPR methods,[3,11] and the Q_A and Q_B sites have been among the most thoroughly explored by EPR techniques.[10−16] To observe the SQ signals directly by these techniques it is necessary to replace the native high spin Fe^{2+} with Zn^{2+}, which does not perturb the function of the acceptor quinones.[11,12]

Structural information about the SQs and their interactions with protein and solvent has mainly been obtained from proton ENDOR spectra in frozen solutions. Three classes of protons can contribute to the spectra: (i) nonexchangeable protons of substituents (isoprene chain, two methoxy groups, and a methyl group), (ii) exchangeable protons forming H-bonds to the quinone oxygens, and (iii) protons associated with the protein or solvent in the immediate vicinity. The major limitation of one-dimensional ENDOR spectroscopy, particularly for ubiquinones, is the large number of protons contributing to the spectra, with fully or partially overlapping frequencies,[11] and the lack of an effective analysis of one-dimensional powder spectra in this situation. To address this, elaborate sample preparations have been required, involving combinations of fully protonated/deuterated protein with protonated/deuterated quinone. As a result, the hyperfine (and nuclear quadrupole) tensors in *Rba. sphaeroides* have been determined only for two protons (deuterons) H-bonded with the carbonyl oxygens of the Q_A SQ, using orientation-selected ^1H and ^2H Q-band ENDOR.[12]

An alternative approach is the recently developed two-dimensional (2D) ESEEM spectroscopy, also called HYSCORE.[17] ^1H HYSCORE spectroscopy allows additional resolution by spreading out peaks that overlap in 1D spectra into 2D in the form of off-diagonal cross-peaks. This technique effectively resolves protons with substantially different anisotropic tensors, although complications remain for protons with close hyperfine couplings in X-band powder spectra.

We have previously used X-band HYSCORE to explore the structural neighborhood of the ubisemiquinones stabilized at the Q_i site of the bc_1 complex of *Rba. sphaeroides*[18] and the Q_H site of the *E. coli* cytochrome bo_3 ubiquinol oxidase.[19] These studies have shown that X-band ^1H HYSCORE spectra together with solvent deuterium exchange readily separate the cross-peaks of exchangeable hydrogen-bonded protons from the lines of non-exchangeable protons and allow quantitative analysis for determinations of the isotropic and anisotropic components of the hyperfine tensors. These parameters, especially when combined with couplings with nitrogen donors, can be used for the computational construction of structural models.[20]

In this article we describe 1D and 2D ESEEM studies of the Q_A and Q_B SQs in reaction centers from *Rba. sphaeroides*. The work has three aims:

First, we demonstrate the resolution of powder ^1H HYSCORE spectra by analyzing model spectral simulations for two protons hydrogen-bonded to the Q_A SQ possessing anisotropic components of the hyperfine tensor that differ by only ∼10%, using the Q-band ENDOR derived tensors.[12] We then show the consistency between data for the Q_A SQ from orientation-selected Q-band ENDOR[12] and from powder X-band 2D ESEEM used in this work, despite partial overlap of individual cross-features from the two protons.

Second, we provide a quantitative characterization of the hyperfine tensors of exchangeable protons around the SQ in the Q_B site of the reaction center. The structural symmetry between the quinone sites allows the findings in the model Q_A SQ study to guide the analysis of the Q_B site, where a larger number of exchangeable protons contributes to the spectra.

Third, we utilize QM/MM calculations on a Q_B site model to assign the observed hyperfine tensors to specific hydrogen bond interactions in the Q_B site, and we compare this with the situation in the Q_A site. The QM/MM simulations also show a difference in the asymmetry of unpaired spin density distribution between the Q_A and Q_B sites, in agreement with available experimental data.

The hyperfine tensors for the exchangeable protons provide a conclusive picture of the hydrogen bond network with the carbonyls of the SQ in the Q_B site. Previously, even the number of hydrogen bonds and the strength of coupling to the Q_B SQ were uncertain, which has frustrated the critical analysis of the spin density distribution and simulations exploiting different structural models.

EXPERIMENTAL SECTION

Sample Preparations. In order to isolate SQ EPR signals, the native, high spin Fe^{2+} must be replaced by diamagnetic Zn^{2+}. Procedures for biochemical metal exchange, along with the methods of bacterial cell

growth and RC isolation, were as previously described.[21] To eliminate cross suppression effects in the HYSCORE spectra and to facilitate resolution of the proton signals (see also Results), RCs were uniformly ^{15}N-labeled. ^{15}N enrichment of RCs was accomplished during cell growth by using ^{15}N-labeled ammonium sulfate (Cambridge Isotopes) in the growth medium. Prior to EPR sample generation, the detergent LDAO, used in RC isolation, was exchanged for Triton X-100 by diluting approximately 100-fold and reconcentrating. Samples with Q_A^- were made by chemical reduction with 8 mM Na-dithionite. For samples with Q_B^- the RCs were combined with a 3-fold excess of both cytochrome *c* and ubiquinone-10. To trap the Q_B SQ, the sample was illuminated by a single laser flash at 532 nm and immediately frozen in liquid nitrogen. Routine optical assay of Fe/Zn-exchanged RC preparations showed a minimum of 80% reconstitution of Q_B activity. However, pulse EPR measurements showed no sign of Q_A SQ signals in Q_B SQ samples in either ^{1}H-HYSCORE (this work) or in ^{14}N- or ^{15}N-HYSCORE,[21] indicating that the functional reconstitution was complete, probably because of the much higher concentrations involved.

EPR and ESEEM Experiments. The instrumentation for X-band and Q-band CW EPR measurements was as previously described.[21] The instrumentation, pulse sequences, and spectral processing for X-band 1D 4-pulse ESEEM ($\pi/2$-τ-$\pi/2$-t-π-t-$\pi/2$-echo) and 2D 4-pulse ESEEM (HYSCORE) ($\pi/2$-τ-$\pi/2$-t_1-π-t_2-$\pi/2$-echo) were also as described.[18,19,21] Spectral simulations were carried out using PC software developed by Dr. Alexei Tyryshkin (now at Princeton University).[21]

Computational Studies. Starting with the *Rba. sphaeroides* structure of Axelrod et al.[8] (PDB 1dv3), we created a model of the Q_B site. This model consisted of L subunit residues 177−242, and M subunit residues 218−220, 233−235, and 265−267 plus the nonheme Fe^{2+}. Hydrogens were added, and the native Fe^{2+} ion was replaced by Zn^{2+}. The ubiquinone isoprene chain was reduced to CH_2CHCH_2. For the optimization studies, two-layer ONIOM calculations ONIOM(B3LYP/6-31G(d):UFF) were performed. The QM layer contained the ubisemiquinone Q_B, His-L190, Gly-L225, Ile-L224, Ser-L223, Zn, and its other ligands. The remaining atoms formed the MM layer. Linking between the QM and MM layers was achieved using hydrogen link atoms. Keeping all heavy atoms except the semiquinone fixed, we optimized the semiquinone geometry within the site. All hydrogen atom positions were optimized. Charges for the MM layer were generated using the qEq method and electrostatic embedding, i.e., ONIOM-EE was employed.[22] This geometry was then used in a further single point ONIOM(B3LYP/EPR-II:UFF) calculation to obtain spin densities and hyperfine couplings. For the Zn atom the 6-31G(d) basis set was used. All calculations were performed using Gaussian 03 software.[23]

SPECTROSCOPIC BACKGROUND

Orientationally Disordered ^{1}H HYSCORE Spectra and Their Analysis. In this work, the proton environment of the SQs is best probed by the 2D ESEEM (HYSCORE) experiment.[17] The essential advantage of the HYSCORE technique is the creation, in 2D spectra, of off-diagonal cross-peaks whose coordinates are nuclear frequencies from opposite electron spin manifolds. The cross-peaks significantly simplify the analysis of congested spectra by correlating the nuclear frequencies of individual nuclei. In addition, HYSCORE separates overlapping peaks along a second dimension and enhances the signal-to-noise ratio through a second Fourier transform. HYSCORE is also very valuable for the detection of extended, anisotropic, "ridge-like" features of low intensity, which are not seen in 1D ESEEM spectra.[24−26]

A nucleus with $I = 1/2$, such as ^{1}H, has two hyperfine nuclear frequencies, ν_α and ν_β, corresponding to two states $m_s = \pm 1/2$ of the electron spin system in the applied magnetic field. In HYSCORE, these may produce a pair of cross-features, (ν_α, ν_β) and (ν_β, ν_α).

The X-band (~9.7 GHz) EPR spectrum of a SQ is usually a single line with width ~0.8 mT.[11] This width is comparable with the excitation width of the microwave pulses, and the spectra obtained can be considered to be powder-type 1D or 2D ESEEM spectra because the resulting pattern contains contributions from all possible orientations of the SQ relative to the applied magnetic field. Orientationally disordered (i.e., powder) HYSCORE spectra of $I = 1/2$ nuclei reveal, in the form of cross-ridge projections, the interdependence of ν_α and ν_β belonging to the same orientations, and analysis of the ridges allows for direct, simultaneous determination of the nuclear isotropic and anisotropic components of the hyperfine tensor.[27]

The contour line shape of the cross-ridge in the powder 2D spectrum of a ^{1}H nucleus, for hyperfine interactions with the axially symmetric tensor $(a - T, a - T, a + 2T)$, is described[27] by eq 1:

$$\nu_\alpha^2 = Q_\alpha \nu_\beta^2 + G_\alpha \quad (1)$$

where $Q_\alpha = ((T + 2a - 4\nu_H)/(T + 2a + 4\nu_H))$ and $G_\alpha = 2\nu_H((4\nu_H^2 - a^2 + 2T^2 - aT)/(T + 2a + 4\nu_H))$ and ν_H is the ^{1}H Zeeman frequency. For each cross-feature, the frequency values along the ridge can be plotted as ν_α^2 versus ν_β^2, transforming the contour line shape into a straight line segment whose slope and intercept are proportional to Q_α and G_ω, respectively. These values can then be used to obtain two possible solutions of isotropic (a) and anisotropic (T) couplings with the same value of $|2a + T|$ and interchanged $A_\perp = |a - T|$ and $A_{||} = |a + 2T|$.[27]

Analysis of the HYSCORE Spectra Simulated Using ENDOR Data for the Q_A Semiquinone. Orientation-selected Q-band ENDOR experiments with fully deuterated RC from *Rba. sphaeroides* in ^1H_2O buffer have provided the hyperfine tensors for two protons participating in H-bonds with O_1 and O_4 of the Q_A semiquinone.[12] The principal values of the anisotropic hyperfine tensors and isotropic couplings determined for these protons are summarized in Table 1. It is clear that the ENDOR data show one proton (H1) to possess a purely axial anisotropic tensor. For the second proton (H2), the rhombicity is only ~4%, and it too can be considered axial for spectral estimates. Table 2 shows the hyperfine tensors and nuclear frequencies for α and β manifolds assuming axial symmetry for both H1 and H2. These

Table 1. ENDOR Determined Hyperfine Tensors (MHz) for Hydrogen-Bonded Protons H1 and H2 in the Q_A Site of the Reaction Center from *Rba. sphaeroides* R-26 (from refs 12 and 13)

proton	H-bond	T_{33}	T_{22}	T_{11}	a	exchange rate
H1	O_4−His (M219)	10.43	−5.23	−5.20	−1.28	slow
H2	O_1−Ala (M260)	9.12	−4.75	−4.37	−0.17	fast

Table 2. ENDOR Derived Hyperfine Frequencies[a] in the Axial Approximation (MHz) for Protons H1 and H2 (from ref 12)

proton	H-bond	$A_\perp = a - T$	$A_{||} = a + 2T$	$\nu_{\alpha||}$	$\nu_{\beta||}$	$\nu_{\alpha\perp}$	$\nu_{\beta\perp}$
H1	O_4−His (M219)	−6.50	9.15	19.29	10.15	11.47	17.97
H2	O_1−Ala (M260)	−4.73	8.95	19.2	10.24	12.36	17.08

[a] Hyperfine frequencies were calculated for proton Zeeman frequency ν_H = 14.73 MHz.

dx.doi.org/10.1021/ja2001538 |*J. Am. Chem. Soc.* 2011, 133, 5525–5537

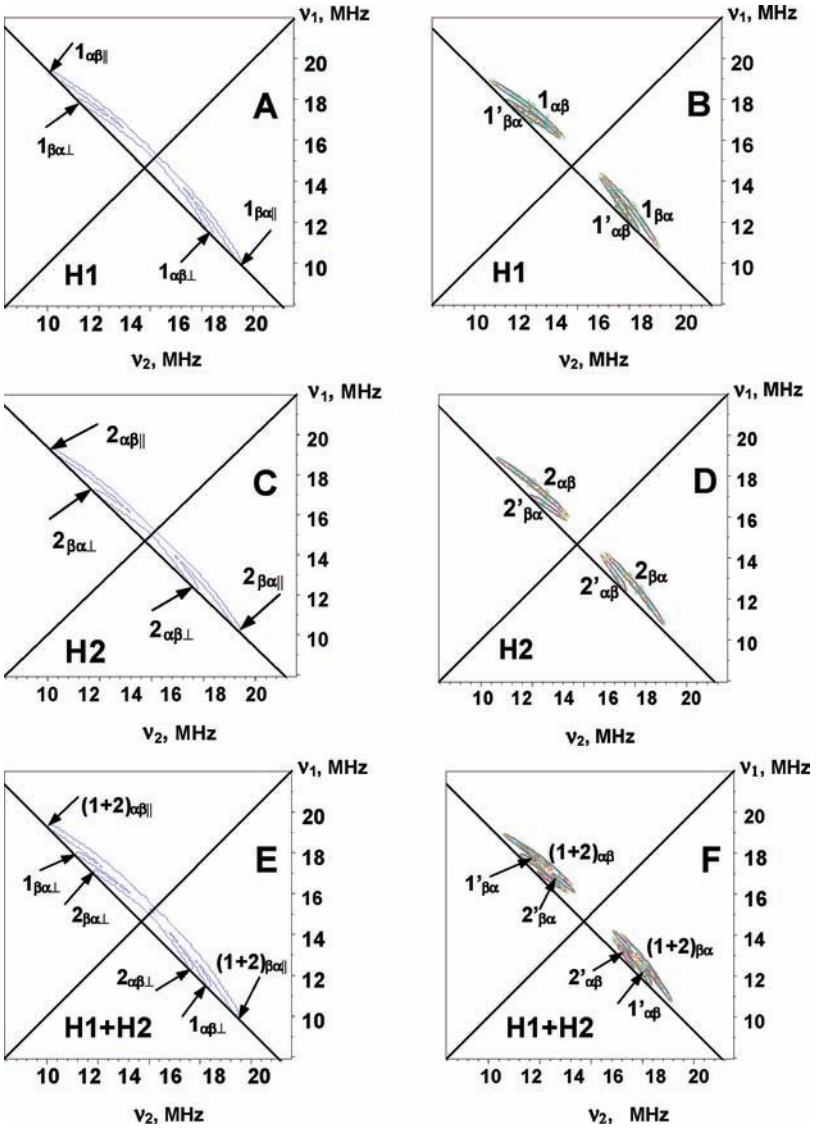

Figure 2. HYSCORE spectra for protons H1 and H2 identified by ENDOR. Left column (A, C, E): contour presentation of the full cross-peaks. Right column (B, D, F): calculated HYSCORE spectra using Q-band ENDOR derived hyperfine tensors shown in Tables 1 and 2, and time between first and second microwave pulses τ = 136 ns. ^{1}H Zeeman frequency is 14.73 MHz (see also text). The spectra qualitatively demonstrate the relative intensity of different ridges. The wider and more extended ridges possess greater intensity.

tensors support the previous assignment of the three couplings A_1 = 4.7 MHz, A_2 = 6.3 MHz, and A_3 = 9.0 MHz (±0.1 MHz) observed in powder ENDOR spectra, to two $A_\perp$ and one $A_\parallel$.[11] The latter represents the overlap of two lines, with the predicted difference between $A_\parallel$ for the two protons on the order of ~0.2 MHz (Table 2). Monitoring the time dependence of the ENDOR line intensities, following substitution of ^1H_2O by ^2H_2O with fully protonated and fully deuterated RCs, confirmed that the three observed couplings belong to two protons. The $^1H/^2H$ exchange times for the protons of the Q_A SQ were found to be $\tau_1 \approx 50$ min and $\tau_2 \approx 1200$ min in protonated RCs and $\tau_1 \approx 10$ min and $\tau_2 \approx 90$ min in fully deuterated RCs.[13]

On the other hand, for the Q_B SQ, couplings assigned to three exchangeable protons were detected by ENDOR, but their hyperfine tensors were not characterized.[10]

To illustrate the characteristics of powder ^{1}H HYSCORE and to identify the complications that arise when the spectra result from more than one nucleus (especially with similar hyperfine couplings), we use the ENDOR data for the Q_A SQ to generate simulated HYSCORE spectra for model analysis. Figure 2 shows, for two protons with principal values of the hyperfine tensors and corresponding nuclear frequencies provided in Tables 1 and 2, an idealized contour presentation of the powder HYSCORE spectra (A, C, E), and the corresponding calculated HYSCORE spectra, with time τ = 136 ns between first and second microwave pulses (B, D, F). The idealized presentation just shows the location of full cross-ridges determined by the hyperfine parameters, as described by eq 1. The calculated spectra take into account suppression effects and show the distribution of intensity along the ridges, which depends on the selected time τ as determined by the intensity coefficient $\sin(\pi\nu_\alpha\tau)\cdot\sin(\pi\nu_\beta\tau)$.[28,29] For each proton (H1, H2) there are two cross-ridges with permutated coordinates, (ν_α, ν_β) or (ν_β, ν_α), extending between $(\nu_{\alpha(\beta)||}, \nu_{\beta(\alpha)||})$ and $(\nu_{\alpha(\beta)\perp}, \nu_{\beta(\alpha)\perp})$. These are located symmetrically on

dx.doi.org/10.1021/ja2001538 |J. Am. Chem. Soc. 2011, 133, 5525–5537

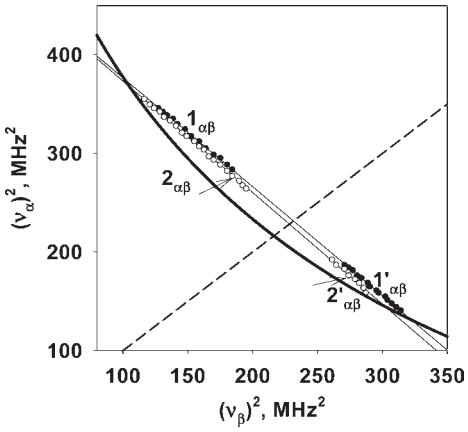

Figure 3. Plots of cross-peaks from the calculated HYSCORE spectra of Figure 2 in the ν_α^2 vs ν_β^2 coordinate system (see text for detailed explanations). The straight lines show the linear fit of plotted data points. The thick curved line is defined by $|\nu_\alpha + \nu_\beta| = 2\nu_H$ with proton Zeeman frequency 14.73 MHz. The dashed line corresponds to the diagonal of the full spectra.

both sides of the diagonal of the 2D spectrum and pass through the diagonal in the idealized presentation. The branches of the two ridges on the same side of the diagonal are located close to each other. In the calculated spectra, the cross-ridges are suppressed in the region of the diagonal. This effectively leads to the appearance of two isolated subridges, $\mathbf{1}_{\alpha\beta}$ and $\mathbf{1}'_{\alpha\beta}$, and $\mathbf{2}_{\alpha\beta}$ and $\mathbf{2}'_{\alpha\beta}$, for H1 and H2, respectively. These subridges can be correlated to each other using a linear regression approach based on eq 1 and illustrated below. Also shown is a superposition of the spectra from two protons in both presentations (Figure 2E, F). The $\nu_{\alpha\|}$ and $\nu_{\beta\|}$ frequencies are very close for both protons (Table 2). As a result, the upper parts of the ridges $\mathbf{1}_{\alpha\beta(\beta\alpha)}$ and $\mathbf{2}_{\alpha\beta(\beta\alpha)}$ are practically indistinguishable in the spectrum and are seen as one ridge $(\mathbf{1} + \mathbf{2})_{\alpha\beta(\beta\alpha)}$. However, the presence of two protons can be recognized from the subridges $\mathbf{1}'_{\alpha\beta(\beta\alpha)}$ and $\mathbf{2}'_{\alpha\beta(\beta\alpha)}$ located near the antidiagonal and corresponding to orientations approaching 90° between the magnetic field and the unique axis of the hyperfine tensor.

We illustrate the approach for determining the hyperfine tensor components by exploring the simulated HYSCORE spectra of Figure 2. The coordinates ν_1 and ν_2 of arbitrary points along cross-ridges were measured from the HYSCORE spectra calculated separately for H1 and H2 (Figure 2B, D) and plotted as sets of values in ν_α^2 vs ν_β^2. Figure 3 shows the plots where the larger frequency ν_1 of each point from subridges $\mathbf{1}_{\alpha\beta}$ and $\mathbf{2}_{\alpha\beta}$ was arbitrarily selected as ν_α, and the smaller frequency ν_2 as ν_β. In contrast, for subridges $\mathbf{1}'_{\alpha\beta}$ and $\mathbf{2}'_{\alpha\beta}$, on the opposite side of the diagonal, the smaller coordinates should be assigned to ν_α and the larger ones to ν_β. This selection places the cross-ridges $\mathbf{1}_{\alpha\beta}$,$\mathbf{2}_{\alpha\beta}$ and $\mathbf{1}'_{\alpha\beta}$,$\mathbf{2}'_{\alpha\beta}$ on opposite sides of the graph relative to the dashed line corresponding to the diagonal in the spectra in Figure 2. In such a presentation, the points from $\mathbf{1}_{\alpha\beta}$ and $\mathbf{1}'_{\alpha\beta}$ fit the linear regression well, thus confirming that they are two parts of the same ridge from proton H1. The same is true for subridges $\mathbf{2}_{\alpha\beta}$ and $\mathbf{2}'_{\alpha\beta}$ from proton H2. The slopes and intercepts for the linear regressions shown in Figure 3 are presented in Table 3, together with two possible sets of (a, T) satisfying eq 1 for protons H1 and H2, and $A_\perp$ and $A_{||}$ values. The curve $|\nu_\alpha + \nu_\beta| = 2\nu_H$ (with ν_H =14.73 MHz, corresponding to the proton Zeeman frequency in a field of 346 mT) is also plotted in Figure 3 to explain the nature of the two solutions determined by eq 1. The points at which this curve crosses each extrapolated straight line correspond to the nuclear frequencies ($\nu_{\alpha||}$, $\nu_{\beta||}$) or ($\nu_{\alpha\perp}$, $\nu_{\beta\perp}$). There are two possible assignments of the parallel or perpendicular orientations for each point and, consequently, two sets of hyperfine tensors, one for each assignment. In this approach, the hyperfine couplings are identical to those determined from the slope and intercept. From the two solutions, one (marked by bold font in Table 3) gives a and T values close to the ENDOR-derived values. In addition, Table S1 in Supporting Information shows that accurate estimates of the hyperfine tensors for H1 and H2 can be obtained from linear fitting of the $\mathbf{1}'_{\alpha\beta}$ and $\mathbf{2}'_{\alpha\beta}$ subridges only. This is especially important when the extended subridges $\mathbf{1}_{\alpha\beta}$ and $\mathbf{2}_{\alpha\beta}$ are not individually resolved.

RESULTS

Quantitative information about the proton environment around the SQ in the Q_A and Q_B sites of RC was obtained from 2D ESEEM (HYSCORE) experiments, because the simpler 1D approaches do not provide the necessary resolution of the multinuclear contributions from protons. In our studies of protons we used uniformly ^{15}N-labeled protein, because the ^{14}N nuclei of atoms hydrogen-bonded with carbonyl oxygens of the SQs produce deep ESEEM, especially for the Q_A SQ (Figure S1 in Supporting Information). ^{14}N ESEEM completely suppressed the proton peaks in HYSCORE spectra of the Q_A SQ due to the cross-suppression effect.[30,31] The ^{15}N nucleus, with spin $I = 1/2$ and no nuclear quadrupole moment, produces a modulation of the echo amplitude that is shallower than the ^{14}N isotope. This allows the appearance of the proton peaks in HYSCORE spectra of the Q_A SQ. For the Q_B SQ in the RC sample with natural abundance ^{14}N, the proton HYSCORE peaks are observed, but ^{15}N labeling further improves the intensity and resolution of the proton spectra. The ^{14}N and ^{15}N X-band HYSCORE spectra of the Q_A and Q_B semiquinones are clearly different (see Figure S2 in Supporting Information, and ref 21) allowing one to draw convincing conclusions about the purity of the preparations containing Q_A or Q_B SQ.

Q_A Semiquinone ^{1}H HYSCORE. The time, τ, which is kept constant in each individual experiment, influences the HYSCORE spectrum by modulating the intensity of cross-peaks. Therefore, measurements were performed at several values of τ to ensure that all cross-peaks were observed. Figure 4 shows the contour and 3D-like stacked presentations of the ^{1}H spectra recorded with τ = 136 ns for the Q_A SQ prepared in ^1H_2O and ^2H_2O buffer. To provide a better view of the different spectral features, in this figure (and others discussed below) only the half of the contour spectrum above the diagonal is shown. In addition, the sum of three spectra recorded with τ = 136, 200 and 400 ns in similar presentations is shown in Figure S3 in Supporting Information to ensure adequate representation of all peaks. No new peaks appear in the sum spectrum although the relative intensities of the different peaks are changed. (Other views and presentations of the Q_A SQ spectra are provided in Supporting Information, Figure S4.)

The spectrum in Figure 4 shows up to four pairs of resolved cross-ridges with different lengths and intensities located symmetrically relative to the diagonal. They are designated $\mathbf{1}_A$, $\mathbf{2}_A$, $\mathbf{3}_A$, and $\mathbf{4}_A$. The peaks or ridges of $\mathbf{1}_A$, $\mathbf{2}_A$, and $\mathbf{3}_A$ deviate from the antidiagonal, indicating a significant anisotropic component (see full spectrum in Figure S3 in Supporting Information). In contrast, cross-peaks $\mathbf{4}_A$ are approximately normal to the diagonal, suggesting smaller anisotropy.[24,25,27]

dx.doi.org/10.1021/ja2001538 |J. Am. Chem. Soc. 2011, 133, 5525–5537

Table 3. Parameters Derived from Contour Lineshape Analysis of the Simulated HYSCORE Spectrum in Figure 2

proton	Q_α	G_α, MHz^2	$(a, T)^1$, MHz	$A_\perp = a - T$, MHz	$A_\parallel = a + 2T$, MHz
H1 (ridges $\mathbf{1}_{\alpha\beta}$, $\mathbf{1}'_{\alpha\beta}$)	−1.10 (0.002)	487.0 (0.5)	∓4.04, ± 5.17	∓9.2	±6.3
			∓1.13, ± 5.17	**∓6.3**	**±9.2**
H2 (ridges $\mathbf{2}_{\alpha\beta}$, $\mathbf{2}'_{\alpha\beta}$)	−1.13 (0.004)	486.4 (0.8)	∓4.13, ± 4.65	∓8.8	±5.2
			∓0.52, ± 4.65	**∓5.2**	**±8.8**

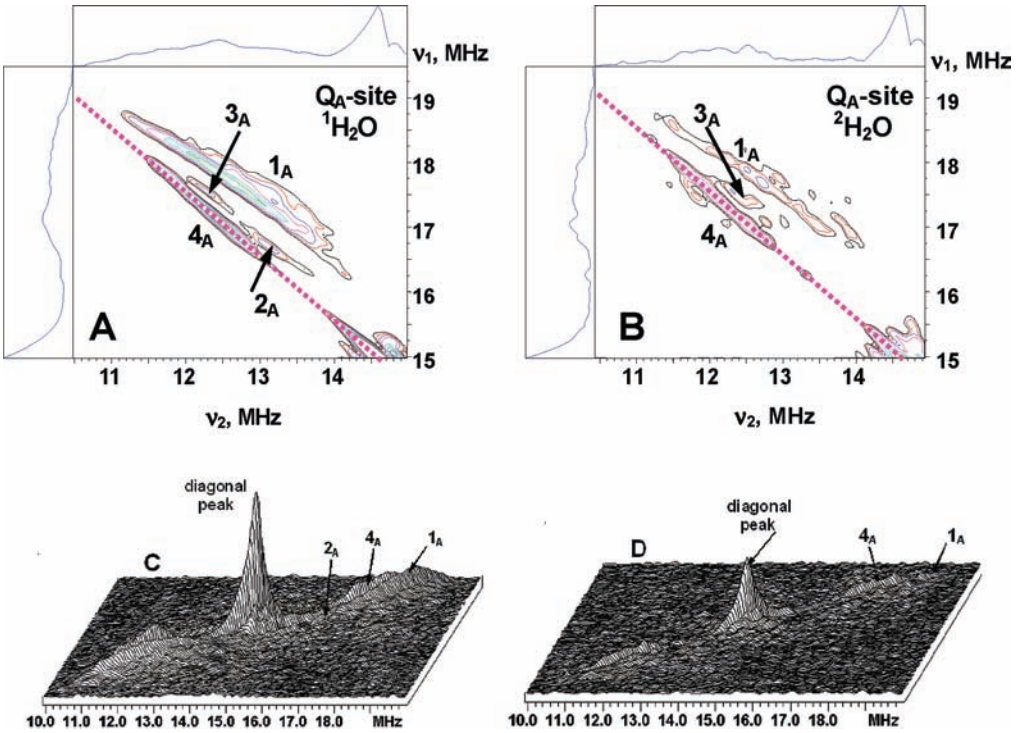

Figure 4. Contour (A, B) and stacked (C, D) presentations of the experimental ^{1}H HYSCORE spectra of the Q_A SQ of *Rba. sphaeroides* reaction centers prepared in ^1H_2O and ^2H_2O (magnetic field 345.9 mT (^1H_2O) and 346.0 mT (^2H_2O), time between first and second pulses τ = 136 ns, microwave frequency 9.702 GHz (^1H_2O) and 9.707 GHz (^2H_2O)). In the stacked presentation, in ^1H_2O, peak $\mathbf{3}_\mathbf{A}$ is hidden between ridges $\mathbf{1}_\mathbf{A}$ and $\mathbf{4}_\mathbf{A}$.

The intensity of cross-ridges $\mathbf{1}_\mathbf{A}$ and $\mathbf{3}_\mathbf{A}$ (Figure 4) is substantially decreased in the HYSCORE spectra obtained under the same conditions but with the sample incubated in ^2H_2O. The remaining ridge $\mathbf{1}_\mathbf{A}$ is also significantly narrower. Cross-peak $\mathbf{2}_\mathbf{A}$ (Figure 4) completely disappeared in this HYSCORE spectrum showing that it is produced by exchangeable proton(s). The same conclusion is probably applicable to cross-features $\mathbf{1}_\mathbf{A}$ and $\mathbf{3}_\mathbf{A}$, taking into account the significantly different exchange rates for the two exchangeable protons H1 and H2 obtained in ENDOR experiments on the Q_A SQ. The remaining signals, therefore, could be assigned to the residue of slowly exchanging proton H1. The intensities of the diagonal peak and its shoulders spread along the antidiagonal (Figure 4C, D) are also partially suppressed in this spectrum, indicating contributions from weaker coupled exchangeable protons. Nevertheless, cross-peak $\mathbf{4}_\mathbf{A}$ and the diagonal peak, with its shoulders, still appear in all spectra, indicating contribution from protons of the SQ substituents and nonexchangeable protons of the protein environment.

The HYSCORE spectra simulated using the ENDOR data (Figure 2) suggest that cross-ridge $\mathbf{1}_\mathbf{A}$ is the overlap of two cross-ridges, $\mathbf{1}_{\alpha\beta}$ and $\mathbf{2}_{\alpha\beta}$, from protons H1 and H2, i.e., $(\mathbf{1} + \mathbf{2})_{\alpha\beta}$. Then

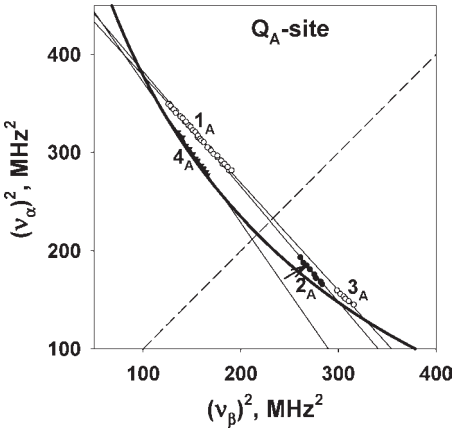

Figure 5. Cross-peaks $\mathbf{1}_\mathbf{A}$–$\mathbf{4}_\mathbf{A}$ from ^{1}H HYSCORE spectrum in Figure 4 plotted in the ν_α^2 vs ν_β^2 coordinate system (see text for detailed explanations). The straight lines show the linear fit of plotted data points. The thick curved line is defined by $|\nu_\alpha + \nu_\beta| = 2\nu_H$ with proton Zeeman frequency 14.73 MHz. The dashed line corresponds to the diagonal of the full spectra.

dx.doi.org/10.1021/ja2001538 |*J. Am. Chem. Soc.* 2011, 133, 5525–5537

cross-peaks $\mathbf{2}_A$ and $\mathbf{3}_A$ correspond to cross-features $\mathbf{2}'_{\beta\alpha}$ and $\mathbf{1}'_{\beta\alpha}$, respectively. These cross-features, defined by local maxima along the ridge, are plotted in ν^2 coordinates according to eq 1 (Figure 5). This presentation clearly shows that the points for $\mathbf{1}_A$ and $\mathbf{3}_A$ as well as $\mathbf{1}_A$ and $\mathbf{2}_A$ fall along two straight lines, indicating the presence of two protons contributing to these three cross-features. Permutation of the larger and smaller coordinates was performed for cross-peaks $\mathbf{2}_A$ and $\mathbf{3}_A$, corresponding to the transformation of the subridges $\mathbf{2}'_{\beta\alpha}$ and $\mathbf{1}'_{\beta\alpha}$ to $\mathbf{2}'_{\alpha\beta}$ and $\mathbf{1}'_{\alpha\beta}$, for correlation with $(\mathbf{1}+\mathbf{2})_{\alpha\beta}$ (see Figure 2F). The cross-features $\mathbf{4}_A$, produced by nonexchangeable protons, possess much smaller hyperfine anisotropy than protons responsible for cross-peaks $\mathbf{1}_A-\mathbf{3}_A$ and do not cross the diagonal. As a result only one cross-feature is used in the linear regression analysis of these points in Figure 5.

Table 4. Characteristics of Hyperfine Tensors of the Protons $H1_A-H3_A$ (MHz) Derived from Experimental HYSCORE Spectra of the Q_A SQ[a,b]

proton(s)	a, T	$A_\perp = a - T$	$A_\parallel = a + 2T$
$H1_A$ (ridges $\mathbf{1}_A$, $\mathbf{3}_A$)	-1.38 ± 0.1, 5.41 ± 0.17	-6.8	9.6
$H2_A$ (ridges $\mathbf{1}_A$, $\mathbf{2}_A$)	-0.17 ± 0.2, 5.07 ± 0.35	-5.2	10
$H3_A$ (ridge $\mathbf{4}_A$)	4.39 ± 0.3, 1.71 ± 0.5	2.7	7.8
$H3_A$ (ridge $\mathbf{4}_A$)[c]	4.0 ± 0.3, 1.6 ± 0.5	2.4	7.2

[a] The subscript A indicates tensor assignments and the corresponding protons from experimental HYSCORE spectra of the Q_A semiquinone, in contrast to the ENDOR-derived tensors for H1 and H2 in Tables 1 and 2. [b] Errors for a and T correspond to 95% prediction intervals for the linear regression results shown in Table S2 in Supporting Information. [c] Sample in ^2H_2O.

Quantitative analysis of the cross-peak contours provides two sets of a and T for exchangeable $H1_A$ (ridges $\mathbf{1}_A$, $\mathbf{3}_A$) and $H2_A$ (ridges $\mathbf{1}_A$, $\mathbf{2}_A$), and nonexchangeable $H3_A$ (ridge $\mathbf{4}_A$) protons (see note to Table 4 regarding subscripts A). The full results of analysis are summarized in Table S2 in Supporting Information. The preferred set (Table 4) was selected on the basis of the ENDOR data, computational works and numerical simulations of HYSCORE spectra (see also Discussion). Particularly, the HYSCORE spectra simulated for $H1_A$ and $H2_A$ using the second solution, with large isotropic constants (Table S2 in Supporting Information), contain only subridges similar to $\mathbf{1}_{\alpha\beta(\beta\alpha)}$ and $\mathbf{2}_{\alpha\beta(\beta\alpha)}$ in Figure 2 while subridges $\mathbf{1}'_{\alpha\beta(\beta\alpha)}$ and $\mathbf{2}'_{\alpha\beta(\beta\alpha)}$ are absent, in contrast to the experimental spectra and the spectra simulated with the preferred parameter set.

Q_B Semiquinone ^{1}H HYSCORE. Figure 6 shows contour (A) and stacked (C) presentations of the ^{1}H HYSCORE spectrum of the Q_B SQ prepared in ^1H_2O buffer, obtained as the sum of three spectra recorded with τ = 136, 200, and 400 ns. We use this presentation because not all cross-peaks possess observable intensity in the spectra at a single value of τ (see Figure S4 in Supporting Information for comparison).

Six pairs of cross-features $\mathbf{1}_B-\mathbf{6}_B$ can be identified in the spectrum. The cross-ridge $\mathbf{1}_B$ shows similar length and deviation from the antidiagonal as cross-peak $\mathbf{1}_A$ in the spectrum of the Q_A SQ although the width and intensity of the ridge are smaller than in the Q_A SQ spectrum. Using both contour and stacked spectra, careful examination of the line-shape for the cross-feature most closely approaching $\mathbf{1}_B$ indicates that it is formed by the overlap of two ridges, marked $\mathbf{2}_B$ and $\mathbf{3}_B$, from two different nuclei (this is also suggested by the 4-pulse ESEEM spectra discussed below). All three cross-features $\mathbf{1}_B-\mathbf{3}_B$ completely disappeared in the

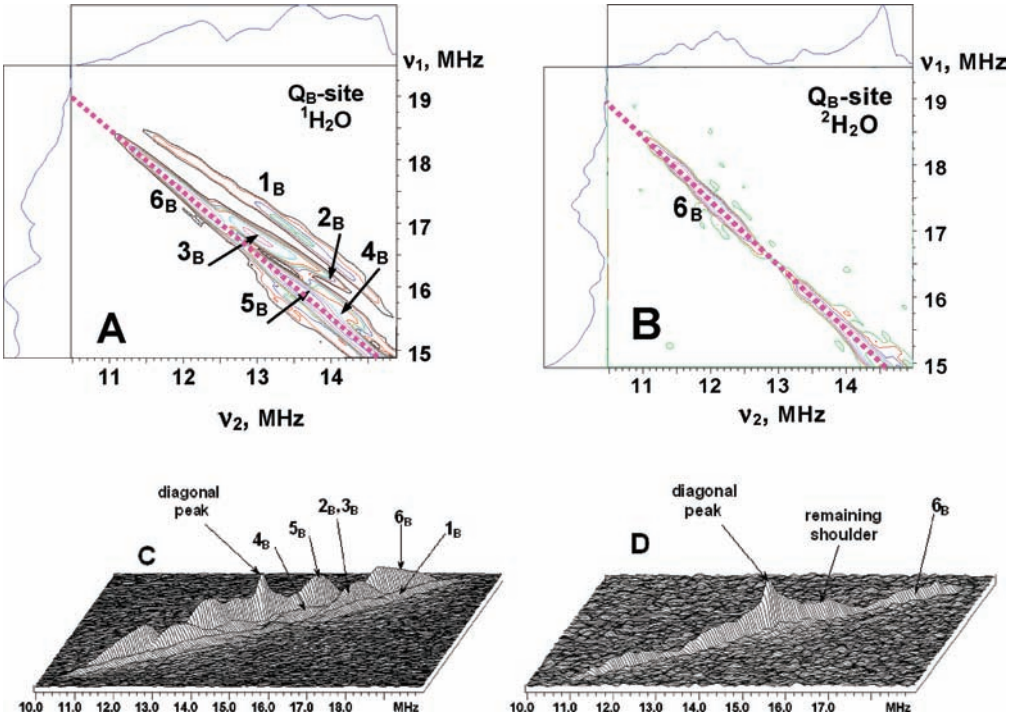

Figure 6. Contour (A, B) and stacked (C, D) presentations of the experimental ^{1}H HYSCORE spectra of the Q_B SQ of *Rba. sphaeroides* reaction centers prepared in ^1H_2O and ^2H_2O. Spectra were obtained as a sum of three individual spectra recorded with time between first and second pulses τ = 136, 200, and 400 ns, (magnetic field 345.1 mT (^1H_2O) and 344.6 mT (^2H_2O), microwave frequency 9.680 GHz (^1H_2O) and 9.666 GHz (^2H_2O)).

dx.doi.org/10.1021/ja2001538 |*J. Am. Chem. Soc.* 2011, 133, 5525–5537

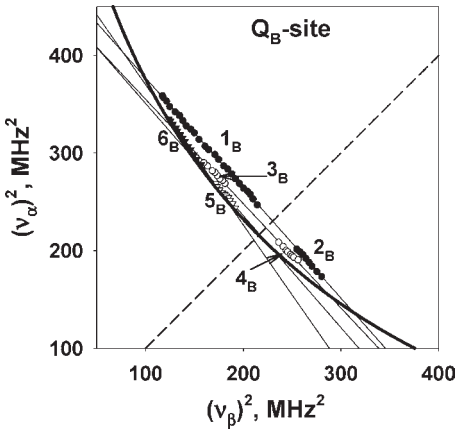

Figure 7. Cross-peaks $\mathbf{1_B}-\mathbf{6_B}$ from ^{1}H HYSCORE spectrum in Figure 6 plotted in the ν_α^2 vs ν_β^2 coordinate system (see text for detailed explanations). The straight lines show the linear fit of plotted data points. The thick curved line is defined by $|\nu_\alpha + \nu_\beta| = 2\nu_H$ with proton Zeeman frequency 14.73 MHz. The dashed line corresponds to the diagonal of the full spectra.

Table 5. Characteristics of Hyperfine Tensors of Protons $H1_B-H4_B$ (MHz) Derived from Experimental HYSCORE Spectra of the Q_B SQ[a,b]

proton	a, T	$A_\perp = a - T$	$A_\parallel = a + 2T$
$H1_B$ (ridges $\mathbf{1_B}$, $\mathbf{2_B}$)	-0.83 ± 0.08, 5.2 ± 0.16	-6.0	9.6
$H2_B$ (ridges $\mathbf{3_B}$, $\mathbf{4_B}$)	-0.88 ± 0.14, 3.71 ± 0.26	-4.6	6.5
$H3_B$ (ridges $\mathbf{5_B}$)	1.09 ± 0.35, 1.87 ± 0.6	-0.8	4.9
$H4_B$ (ridges $\mathbf{6_B}$)	4.27 ± 0.25, 1.92 ± 0.35	2.4	8.1
$H4_B$ (ridges $\mathbf{6_B}$)[c]	4.8 ± 0.12, 1.59 ± 0.25	3.2	8.0

[a] The subscript B indicates assignments from experimental HYSCORE spectra of the Q_B semiquinone. [b] Errors for a and T correspond to 95% prediction intervals for the linear regression results shown in Table S3 in Supporting Information. [c] Sample in ^2H_2O.

spectrum of the sample prepared in ^2H_2O buffer, showing their relation to exchangeable protons. The spectrum of the Q_B SQ also shows two cross-peaks $\mathbf{4_B}$ and $\mathbf{5_B}$, for which there are no counterparts in the spectrum of the Q_A SQ. These are also absent in the spectrum after $^1H/^2H$ exchange. Only peak $\mathbf{6_B}$ (similar to peak $\mathbf{4_A}$ in the Q_A SQ spectrum) is still present in the spectrum after $^1H/^2H$ exchange, together with the shoulders of the diagonal ^1H matrix line.

The ν_α^2 versus ν_β^2 plot of the cross-features from the Q_B SQ ^1H HYSCORE spectrum (Figure 7) suggests that $\mathbf{1_B}$ and $\mathbf{2_B}$, and $\mathbf{3_B}$ and $\mathbf{4_B}$ are the subridges of cross-features belonging to two different protons. In terms of the designations used in Figure 2, $\mathbf{1_B}$ and $\mathbf{2_B}$ are similar to subridges $\mathbf{1}_{\alpha\beta}$ and $\mathbf{1'}_{\beta\alpha}$ from proton $H1_B$, and $\mathbf{3_B}$ and $\mathbf{4_B}$ are subridges $\mathbf{2}_{\alpha\beta}$ and $\mathbf{2'}_{\beta\alpha}$ from proton $H2_B$. The subscript B indicates assignments from experimental HYSCORE spectra of the Q_B semiquinone. In agreement with this suggestion $\mathbf{1_B}$ and $\mathbf{2_B}$, and $\mathbf{3_B}$ and $\mathbf{4_B}$ (after permutation of the smaller and larger coordinates for $\mathbf{2_B}$ and $\mathbf{4_B}$ placing them to the opposite side of the spectrum relative to the diagonal), fall well along two straight lines and belong to two exchangeable protons $H1_B$ and $H2_B$ with $T \approx 5.2$ and 3.7 MHz. There are no other cross-features in the spectrum that can be correlated with cross-peaks $\mathbf{5_B}$ and $\mathbf{6_B}$. The characteristics of the slopes and intercepts for the linear regressions shown in Figure 5 are presented in Table S3 in Supporting Information, together with two possible sets of (a, T) that satisfy eq 1. Table 5 shows the preferred sets of the hyperfine couplings.

Sum Combination Peaks in 1D 4-Pulse ESEEM. Additional information about the exchangeable protons, supporting the HYSCORE data, was obtained from the 1D four-pulse ESEEM spectra (Figure 8). These spectra contain lines in the region of the double proton Zeeman frequency ($2\nu_H$, at 29.4 MHz), which are sum-combination harmonics $(\nu_\alpha + \nu_\beta)$ of two basic frequencies ν_α and ν_β. These harmonics are not created in HYSCORE experiments. This approach is particularly useful for the resolution of protons with different anisotropic couplings.[32]

The four-pulse ESEEM spectrum of the Q_A SQ in ^1H_2O buffer contains two well-resolved lines in the region of the proton $2\nu_H$, as shown in Figure 8. The most intense line appears exactly at the $2\nu_H$ frequency and represents the contribution of weakly coupled protons from the protein environment with $(\nu_\alpha + \nu_\beta) \cong 2\nu_H$. The spectrum also reveals a broad, asymmetrical peak of lower intensity shifted from $2\nu_H$ to higher frequencies, with a shoulder on the high-frequency side. This peak does not possess a well-defined maximum and is consistent with two overlapping peaks with shifts of 0.8−1.1 MHz. This feature is greatly diminished in the spectrum of the sample prepared in ^2H_2O, indicating that it contains a major contribution from exchangeable protons.

The four-pulse spectrum of the Q_B SQ shows a single, narrow peak shifted by ~0.9 MHz from $2\nu_H$. In addition, there is a distinct, shoulder-like feature located near the $2\nu_H$ peak. The flat maximum indicates a shift of ~0.25−0.50 MHz. Both features disappear in ^2H_2O.

The shifts observed in the four-pulse ESEEM are well described[32] by eq 2

$$\Delta = 9T^2/16\nu_H \qquad (2)$$

which yields the anisotropic component T for the exchangeable protons producing shifted lines (Table 6). The T values determined from the shifts of the sum-combination lines are consistent with the values obtained from the HYSCORE analysis for Q_A and Q_B site semiquinones. Particularly, $T \approx 4.6-5.4$ MHz was found for the Q_A site. In the Q_B SQ spectrum, the line with the larger shift corresponds to $T \approx 5$ MHz and relates to $H1_B$. The broad feature near the $2\nu_H$ line corresponds to protons with $T < 3.7$ MHz and can be accounted for by contributions of the exchangeable protons $H2_B$ and $H3_B$, which possess significantly lower anisotropic hyperfine coupling than $H1_B$. This contrasts with the Q_A SQ where both detected exchangeable protons, $H1_A$ and $H2_A$, exhibit similar hyperfine tensors.

DISCUSSION

Exchangeable Protons. The principal values of the hyperfine tensors determined in our HYSCORE studies for the exchangeable protons around the Q_A SQ are fully consistent with previously published orientation-selected Q-band ENDOR data[12] but were obtained with considerably greater ease of sample preparation, much shorter data acquisition time, and simpler analysis. We found the presence of two protons $H1_A$ and $H2_A$, with similar anisotropic hyperfine couplings $T \approx 4.6-5.4$ MHz, involved in the O_4−His (M219) and O_1−Ala (M260) hydrogen bonds.

Besides the cross-features assigned to these two protons, $^1H/^2H$ exchange did not result in any other significant loss of spectral intensity in the Q_A SQ spectrum, e.g., in areas remote from the diagonal peak where distant nuclei mostly contribute. This is in agreement with the current vision of the Q_A site where

dx.doi.org/10.1021/ja2001538 |J. Am. Chem. Soc. 2011, 133, 5525–5537

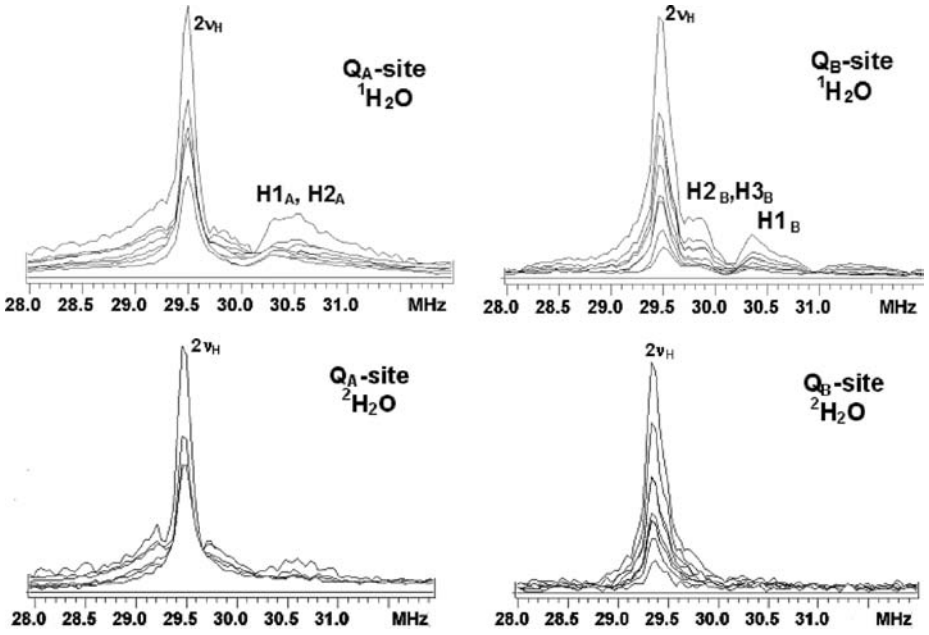

Figure 8. Stacked presentations of sets of four-pulse ESEEM spectra of the Q_A and Q_B SQs in *Rba. sphaeroides* reaction centers prepared in ^1H_2O and ^2H_2O. The spectra show the modulus of the Fourier transform along the time (T) axis for different times between first and second pulses, τ. The initial time τ is 100 ns in the farthest trace and was increased by 12 ns in successive traces. Microwave frequency and magnetic field were 9.711 GHz and 346.2 mT (Q_A in ^1H_2O), 9.705 GHz and 346.0 mT (Q_A in ^2H_2O), 9.708 GHz and 346.1 mT (Q_B in ^1H_2O), and 9.664 GHz and 344.5 mT (Q_B in ^2H_2O).

Table 6. Anisotropic Hyperfine Couplings for Exchangeable Protons in the Q_A and Q_B Sites Estimated from the Shift of the Sum Combination Harmonics

site	shift Δ, MHz	T, MHz
Q_A	0.8−1.1	4.6−5.4
Q_B	0.9−1.0	4.9−5.1
	0.2−0.5	2.3−3.6

only two hydrogen bonds, one to each carbonyl, are responsible for coupling the SQ to the protein.

The HYSCORE spectra of the Q_B SQ have resolved features assigned to exchangeable protons with distinct anisotropic couplings $T \approx 5.2$ MHz and 3.7 MHz. These values exceed the $T \approx 3$ MHz observed for in-plane hydrogen-bonded protons in alcoholic solutions.[33−35] Hydrogen bonding to the quinone carbonyl groups occurs via proton donation to one or both lone pairs on the sp^2-hybridized carbonyl oxygen.[36] Besides these two protons discussed here for the Q_B SQ, we found a marked loss of spectral intensity after $^1H/^2H$ exchange for a peak accompanying the antidiagonal, with a splitting of ∼2.5 MHz (peak $\mathbf{5_B}$). This indicates the presence of an additional exchangeable proton with $T \approx 1.9$ MHz estimated from contour line shape analysis.

As expected from the simulated spectra, the *powder* X-band HYSCORE spectra did not resolve all of the cross-ridges of the Q_A SQ protons, but the linear analysis clearly identified them through the correlations between features (Figure 5). Similarly, the four-pulse ESEEM spectra did not fully separate all the shifted proton sum-combination peaks, due to line broadening, although our model simulations of the four-pulse spectra with ENDOR derived tensors did resolve peaks from two Q_A protons. One likely factor contributing to broadening of the lines and influencing the resolution is the "strain" of the hyperfine parameters, i.e., the static distribution of hyperfine parameters. Analysis

Table 7. SQ Optimized Carbonyl and Hydrogen Bonding Distances in the Q_A and Q_B Sites[a,b]

bond	Q_A site	Q_B site
C_4-O_4	1.29	1.28
C_1-O_1	1.27	1.28
O_4-HN_δ His-M219/L190	1.62	1.58
O_1-HN Ala-M260/Gly-L225	1.84	2.00
O_1-HO Ser-L223		1.81
O_1-HN Ile-L224		2.30

[a] Q_A data taken from ref 20. [b] All distances in angstroms.

of the lineshapes in the "single-crystal-like" Q-band ENDOR spectra from the protons of hydrogen bonds in the Q_A site of RCs from *Rba. sphaeroides*[12] shows that the influence of this factor on the hyperfine coupling value would not exceed ±5%. For couplings of ∼5 MHz, this could give broadening up to 0.5 MHz for basic frequencies and the spread in the position of line maximum for combination harmonics up to 0.3 MHz. In powder spectra such broadening does influence the resolution of the individual lines from protons $H1_A$ and $H2_A$ in the Q_A site.

Assignment of Hyperfine Couplings through QM/MM Calculations. To help assign the observed hyperfine couplings to specific interactions within the Q_A and Q_B sites, we have obtained calculated values using QM/MM density functional theory-based electronic structure calculations. The excellent ability of DFT-based calculations to accurately calculate hyperfine couplings for semiquinone free radicals has been demonstrated some time ago.[37] A recent report has shown how such calculations can be extended to model semiquinone protein binding sites using QM/MM calculations.[20] The carbonyl and hydrogen bonding distances calculated for SQ in the Q_A and Q_B sites are given in Table 7, while the calculated hyperfine

dx.doi.org/10.1021/ja2001538 |*J. Am. Chem. Soc.* 2011, 133, 5525–5537

Table 8. Calculated ^{1}H and ^{14}N Hyperfine Couplings (MHz) for Q_A and Q_B Site Hydrogen Bonding Interactions with SQ

Q_A site[a]			Q_B site		
position	anisotropic T_{33}, T_{22}, T_{11}	isotropic a	position	anisotropic T_{33}, T_{22}, T_{11}	isotropic a
^{1}HN His-M219	10.4	0.6	^{1}HN His-L190	10.2	−0.4
	−5.3			−5.3	
	−5.0			−4.9	
^{1}HN Ala-M260	9.3	−1.8	^{1}HN Gly-L225	6.6	−0.6
	−4.7			−3.7	
	−4.6			−2.9	
			^{1}HN Ile-L224	3.9	−0.1
				−2.1	
				−1.8	
			^{1}HO Ser-L223	7.6	−0.8
				−4.0	
				−3.7	
$^{14}N_{\delta}$ His-M219	0.6	2.6	$^{14}N_{\delta}$ His-L190	0.4	1.5
	−0.3			−0.2	
	−0.3			−0.2	
^{14}NH Ala-M260	0.6	1.5	^{14}NH Gly-L225	0.3	0.6
	−0.3			−0.2	
	−0.3			−0.1	
			^{14}NH Ile-L224	0.2	0.1
				−0.1	
				−0.1	

[a] Q_A data taken from ref 20.

couplings for the exchangeable protons are given in Table 8. For the Q_A site, T ($T = T_{33}/2$) values calculated for the His-M219 $N_{\delta}{}^{1}H$ (5.3 MHz) and Ala-M260 peptide $N^{1}H$ (4.6 MHz) are in very good agreement with the respective T values of 5.2 and 4.6 MHz from Q-band ENDOR[12] and with our HYSCORE results, 5.4 and 5.1 MHz. We can therefore confidently assign the experimental T values to these proton interactions within the Q_A site. In addition the calculated ^{14}N isotropic hyperfine couplings for the His-M219 N_{δ} (2.6 MHz) and the Ala-M260 peptide N (1.5 MHz) are in good agreement with the experimental values of 2.5 and 1.9 MHz estimated from the ^{14}N and ^{15}N HYSCORE spectra of this work (Figure S2 in Supporting Information). A previous two- and three-pulse ESEEM study[14,15] reported hyperfine couplings of 1.8 and 1.1 MHz, which were not assigned to particular nitrogens due to uncertainty in the correlation of the single-quantum and double-quantum transitions from the same nitrogens in 1D ESEEM spectra.

For the Q_B site, the largest ^{1}H tensor component in the calculations gives a value of 5.1 MHz for the coupling between the His-L190 $N_{\delta}H$ group and the O_4 of the SQ (see Table 8). The experimentally observed T value of 5.2 MHz is therefore assigned to this interaction. Furthermore, the calculated ^{14}N isotropic hyperfine coupling for the Q_B site N_{δ} His-L190 is 1.5 MHz, in agreement with the reported experimental value of 1.5 MHz.[21] For the O_1 side in the Q_B site there are three ^{1}H hyperfine couplings calculated; two strong hydrogen bonding interactions, with the OH of Ser-L223 and the peptide NH of Gly-L225, and a weaker dipolar coupling with the peptide NH of Ile-L224. The calculated T value for the Ile-L224 peptide NH (1.95 MHz) is assigned to the experimentally observed T value of 1.9 MHz. The peptide NH of Gly-L225 is calculated to have a ^{14}N isotropic value of 0.6 MHz whereas the corresponding value for Ile-L224 is 0.1 MHz. The experimentally observed ^{14}N isotropic coupling of 0.5 MHz[21] is therefore assigned to the NH Gly L-225 interaction. The much smaller value calculated for Ile-L224 would not be distinguishable from the matrix contributions on the diagonal.

The T values calculated for protons of Ser-L223 (3.8 MHz) and Gly-L225 (3.3 MHz) are both likely to contribute to the experimentally derived T = 3.7 MHz value. The HYSCORE spectra calculated with the hyperfine coupling values for protons of Ser-L223, Gly-L225 and His-L190 from Table 8 showed that the cross-peaks from Ser-L223 and Gly-L225 protons are indistinguishable in the sum spectrum (Figure S7 in Supporting Information, A−F). The addition of the His-L190 proton gives the total spectrum, reproducing the shape of the overlapped cross-features (corresponding to the features assigned to $\mathbf{2_B}$ and $\mathbf{3_B}$ in the experimental spectra in Figure 6 and Figure S5 in Supporting Information) and its location relative to the cross-ridge (equivalent to $\mathbf{1_B}$ in Figure 6 and Figure S5 in Supporting Information) from the His proton (Figure S7 in Supporting Information, G−L). Thus, these calculations qualitatively support the suggested contribution of the Ser-L223 and Gly-L225 protons to the feature with T = 3.7 MHz in the experimental spectra. Further work using orientation-selected Q-band ENDOR or pulsed EPR at lower microwave frequencies is needed to confirm this result experimentally.

Nonexchangeable Protons. The hyperfine couplings of nonexchangeable protons in the Q_A and Q_B semiquinones have been extensively studied by multifrequency (X-, Q-, and W-band) ENDOR in frozen solutions and X-band ENDOR in single-crystals.[11,38,39] These studies reported the couplings for the protons of a rotating methyl group (C_5') and one proton from a methylene group of the isoprenoid chain of Q_A. All

dx.doi.org/10.1021/ja2001538 |J. Am. Chem. Soc. 2011, 133, 5525–5537

Table 9. Calculated ^{13}C, ^{17}O, and ^{1}H Hyperfine Couplings (MHz) for the Q_A and Q_B Semiquinones[a,b]

Q_A site[a]			Q_B site		
position	anisotropic T_{33}, T_{22}, T_{11}	isotropic a	position	anisotropic T_{33}, T_{22}, T_{11}	isotropic a
$^{13}C_1$	20.1	−7.0	$^{13}C_1$	30.6	3.3
	−11.8			−16.6	
	−8.3			−14.0	
$^{13}C_4$	33.1	8.4	$^{13}C_4$	26.3	1.0
	−17.6			−14.4	
	−15.5			−11.9	
$^{17}O_1$	−78.8	−19.9	$^{17}O_1$	−66.9	−18.3
	39.7			−33.6	
	39.1			−33.3	
$^{17}O_4$	−54.0	−16.0	$^{17}O_4$	−62.6	−18.2
	27.3			−31.4	
	26.7			−31.2	
^{1}H $CH_3(5')$	2.4	4.3	^{1}H $CH_3(5')$	2.6	7.6
	−1.6			−1.7	
	−0.8			−1.0	

[a] Q_A data taken from [20] [b] Experimentally determined hyperfine couplings from ref 11: ^{13}C couplings, $A_{obs} = a + T_{33}$; Q_A site, 22.7 MHz (C_1) and 35 MHz (C_4); Q_B site, 27.7 MHz (C_1) and 32.2 MHz (C_4). ^{17}O couplings, $A_{obs} = a + T_{33}$; Q_A site, −94 MHz (O_1) and −75 MHz (O_4); Q_B site, −88 MHz (O_1) and −82 MHz (O_4). Reported couplings for methyl group are summarized in Table S4 in Supporting Information.

experiments with Q_A SQ have consistently shown that the maximum and minimum principal values of the hyperfine tensor are about 6.8 and 3.0 MHz for the methyl protons and 8.8 and 5.0 MHz for the methylene proton (Table S4 in Supporting Information). This suggests that the lines from methyl and methylene protons will partially overlap in powder X-band HYSCORE spectra.

ENDOR studies of the Q_B SQ have reported the coupling for methyl protons only, with larger isotropic coupling than for the Q_A SQ. Q- and W-band studies indicated maximum and minimum principal values of the hyperfine tensor of 7.8 and 3.9 MHz.[11,39]

The HYSCORE spectra of the Q_A and Q_B semiquinones after deuterium exchange show only one pair of cross-peaks, i.e., $\mathbf{4_A}$ and $\mathbf{6_B}$, respectively, along the antidiagonal and well-separated from the diagonal peak and remaining shoulders. Analysis of the contour line-shape of these peaks in the samples prepared in $^{1}H_2O$ and $^{2}H_2O$ gives similar results for both SQs, and with only very minor contributions from exchangeable protons in this vicinity. The formal axial tensors are: (7.2, 2.4, 2.4) MHz with a = 4.0 MHz and T = 1.6 MHz for the Q_A SQ, and (8.0, 3.2, 3.2) MHz with a = 4.8 MHz and T = 1.6 MHz for the Q_B SQ. These values are in reasonable agreement with those derived from ENDOR, although the isotropic contributions are somewhat smaller and the anisotropic components larger ($T \approx 1.1-1.2$ MHz for CH_3 and CH_2 protons). The HYSCORE analysis consequently yields a larger difference between the maximum and minimum principal values of the hyperfine tensors. The difference likely arises from the overlap of the methyl and methylene proton lines, which increases the apparent length of the HYSCORE cross-peak and leads to a larger anisotropic component in the formal analysis.

Proton resonances with smaller splittings have also been observed in ENDOR spectra, but have not been assigned. They should presumably belong to the second proton of the CH_2 group, other protons of the isoprenoid chain, the methoxy groups, and protons from the protein matrix. These protons contribute to the shoulders of the diagonal line in HYSCORE spectra.

From the QM/MM calculations (Table 9), the ^{1}H CH_3 values for Q_A are in good agreement with the experimentally determined values (see also ref 20). For Q_B the calculated isotropic hyperfine coupling is predicted to be larger than that found for Q_A in agreement with the experimental determinations. However, the Q_B value calculated is significantly higher than that observed experimentally, suggesting that the model in its current form overestimates the spin density at C_5 of the Q_B SQ. Since the ^{17}O and ^{13}C coupling values calculated for the carbonyls are in good agreement with experiment, the asymmetry along the C_1-C_4 quinone axis is well reproduced. However, asymmetry across the C_2-C_5 axis could be affected by the torsional angle of the C_2 methoxy group, which we have shown to be absolutely required for Q_B activity.[2,40] Proper understanding of the C_5 spin anomaly will require further knowledge of the unpaired spin density distribution over the ring carbons. This can be obtained from studies of ^{13}C ring-labeled Q_A and Q_B SQs, and such experiments are under consideration.

Asymmetry in Spin Density Distribution. Differences in the hydrogen bonding interactions with the quinone oxygens is expected to lead to asymmetry of the spin distribution in the radical anion. Comparison of the ^{1}H, ^{13}C and ^{17}O couplings for SQ in the Q_A and Q_B sites with those of ubiquinone-10 anion radicals in alcoholic solution led to the conclusion that the Q_A quinone binding site is more asymmetric than the Q_B site.[11] Based on the results and discussion above it can be inferred that the interactions with both SQs at the O_4 atom are similar, where a strong hydrogen bond is formed with the N_δ atom of a histidine residue. The O_1 interactions, however, are significantly different. For the Q_A site only one hydrogen bonding interaction is found with the peptide NH of Ala-M260, whereas in the Q_B site there are interactions with the peptide NH of Gly-L225 and the OH group of Ser-L223, and a weaker interaction with the peptide NH group of Ile-L224.

In the Q_A site, the stronger hydrogen bond to the O_4 oxygen gives rise to an asymmetric spin density distribution for the ubisemiquinone. For the Q_B site, the strong hydrogen bonding

dx.doi.org/10.1021/ja2001538 |J. Am. Chem. Soc. 2011, 133, 5525–5537

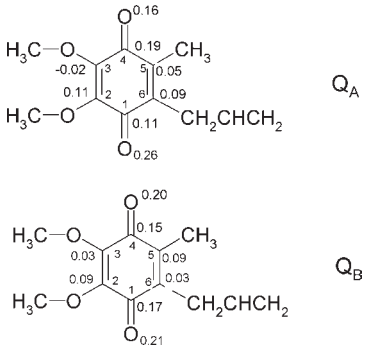

Figure 9. Calculated Mulliken spin populations for the semiquinone in the Q_A and Q_B sites.

interaction to the O4 atom is balanced by the double hydrogen bond interaction at the O_1 atom in addition to a weaker interaction with the NH group of Ile-L224. This leads to a more symmetric spin density distribution for the Q_B SQ as previously indicated by the experimental ^{13}C and ^{17}O hyperfine couplings.[11]

Table 9 gives the calculated isotropic and anisotropic ^{13}C and ^{17}O hyperfine couplings for the Q_A and Q_B SQs. Here the asymmetry difference between the two sites is clearly demonstrated by the large differences in the calculated values of the 1 and 4 positions for the Q_A SQ, whereas similar values are calculated for the Q_B SQ. The calculated total tensors show good agreement with the experimentally determined values of reference provided in the notes to Table 9.[11]

The difference in methyl group hyperfine couplings is another indicator of the different spin density asymmetries exhibited by the Q_A and Q_B SQs. For Q_A, the stronger hydrogen bond at the O_1 atom leads to a low spin density at C_5 (see spin populations in Figure 9), which, in turn, leads to a lower hyperfine coupling for the methyl group protons. For the Q_B SQ, the more symmetric spin density distribution leads to a higher spin density value at C_5, which gives rise to a larger methyl group hyperfine coupling. This is similar to the situation in protic solvents where similar hydrogen bond strengths to each oxygen are expected.

The difference in spin asymmetry for the Q_A and Q_B site semiquinones is well illustrated by the calculated Mulliken spin populations shown in Figure 9, where a much more symmetric spin population is shown for the Q_B SQ. This difference in spin density distribution for the two semiquinones may well contribute to their different functions in electron transfer. The asymmetry of the Q_A site in bacterial RCs polarizes the electron density of the Q_A SQ toward Q_B and it has been suggested that this might contribute to the electron transfer to Q_B.[11] However, in the similar, Type II reaction center of oxygenic photosystem II, the H-bond strengths that are presumed to underlie the spin density asymmetry have been reported to be opposite to that in bacterial RCs, i.e., the interaction with the peptide nitrogen was strongest.[41] Thus, the directional component of the electron distribution in Q_A may not be a design requirement of functional Q_A to Q_B electron transfer. However, the asymmetry will likely affect the redox potential regardless of its particular polarity. For the Q_B site the more symmetric spin density resembles the *in vitro* SQ in protic solvents favoring double reduction and formation of the quinol form. The extra hydrogen bonding interactions found in the Q_B site will also increase the electron affinity of Q_B compared with Q_A, which should lead to a higher redox potential for Q_B, as observed experimentally.[2]

CONCLUSION

We have found that a principal difference between the SQ in the Q_A and Q_B sites of purple bacterial reaction centers is an increased number of hydrogen bond interactions at the O_1 atom for the Q_B SQ. This leads to a symmetric spin density distribution for the Q_B SQ and also an enhanced stabilization. The hydrogen bonding pattern in the binding site is able to control the reduction properties of the quinone. In other type II reaction centers, such as Photosystem II, the hydrogen bonding interactions with the Q_A semiquinone are also highly asymmetrical, suggesting that a similar control mechanism exists.[41] The fine-tuning of SQ properties through hydrogen bonding is likely to be a key mechanism for controlling quinone reduction in biological systems.

ASSOCIATED CONTENT

Supporting Information. Two-pulse ESEEM for Q_A and Q_B SQs, ^{14}N,^{15}N HYSCORE spectra of the Q_A site SQ, additional ^1H HYSCORE spectra for Q_A and Q_B SQs, complete ref 23, additional tables with results of HYSCORE analyses. This material is available free of charge via the Internet at http://pubs.acs.org.

AUTHOR INFORMATION

Corresponding Author
cwraight@illinois.edu; dikanov@illinois.edu; patrick.omalley@manchester.ac.uk

ACKNOWLEDGMENT

This investigation was supported by the NIH GM062954 Grant and DE-FG02-08ER15960 Grant from Chemical Sciences, Geosciences and Biosciences Division, Office of Basic Energy Sciences, Office of Sciences, US DOE (S.A.D.), NSF Grant MCB0818121 (C.A.W.) and NCRR/NIH Grant S10-RR15878 for pulsed EPR instrumentation. P.J.O.M. acknowledges the EPSRC U.K. National Service for Computational Chemistry Software (NSCCS).

REFERENCES

(1) Okamura, M. Y.; Paddock, M. L.; Graige, M. S.; Feher, G. *Biochim. Biophys. Acta* **2000**, *1458*, 148–163.
(2) Wraight, C. A. *Front. Biosci.* **2004**, *9*, 309–337.
(3) Wraight, C. A.; Gunner, M. R. In *The Purple Phototrophic Bacteria*; Hunter, C. N., Daldal, F., Thurnauer, M. C., Beatty, J. T., Eds.; Springer Science + Business Media B.V.: New York, 2009; pp 379−405
(4) Lancaster, C. R. D. *FEBS Lett.* **1998**, *545*, 52–60.
(5) Lancaster, C. R. D.; Ermler, U.; Michel, H. In *Anoxygenic Photosynthetic Bacteria*; Blankenship, R. E., Madigan, M. T., Bauer, C. E., Eds.; Kluwer Academic Publishers: Dordrecht, 1995; pp 503−526.
(6) Xu, Q.; Gunner, M. R. *Biochemistry* **2002**, *41*, 2694–2701.
(7) Stowell, M. H.; McPhillips, T. M.; Rees, D. C.; Soltis, S. M.; Abresch, E.; Feher, G. *Science* **1997**, *276*, 812–816.
(8) Axelrod, H. L.; Abresch, E. C.; Paddock, M. L.; Okamura, M. Y.; Feher, G. *Proc. Natl. Acad. Sci. U.S.A.* **2000**, *97*, 1542–1549.
(9) Koepke, J.; Krammer, E. M.; Klingen, A. R.; Sebban, P.; Ullmann, G. M.; Fritzsch, G. *J. Mol. Biol.* **2007**, *371*, 396–409.
(10) Paddock, M. L.; Flores, M.; Isaacson, R.; Chang, C.; Abresch, E. C.; Okamura, M. Y. *Biochemistry* **2007**, *46*, 8234–8243.
(11) Lubitz, W.; Feher, G. *Appl. Magn. Reson.* **1999**, *17*, 1–48.

(12) Flores, M.; Isaacson, R.; Abresch, E.; Calvo, R.; Lubitz, W.; Feher, G. *Biophys. J.* **2007**, *92*, 671–682.
(13) Flores, M.; Isaacson, R.; Abresch, E.; Calvo, R.; Lubitz, W.; Feher, G. *Biophys. J.* **2006**, *90*, 3356–3362.
(14) Bosch, M. K.; Gast, P.; Hoff, A. J.; Spoyalov, A. P.; Tsvetkov, Yu. D. *Chem. Phys. Lett.* **1995**, *239*, 306–312.
(15) Spoyalov, A. P.; Hulsebosch, R. J.; Shochat, S.; Gast, P.; Hoff, A. J. *Chem. Phys. Lett.* **1996**, *263*, 715–720.
(16) Lendzian, F.; Rautter, J.; Käss, H.; Gardiner, A.; Lubitz, W. *Ber. Bunsenges. Phys. Chem.* **1996**, *100*, 2036–2040.
(17) Höfer, P.; Grupp, A.; Nebenführ, H.; Mehring, M. M. *Chem. Phys. Lett.* **1986**, *132*, 279–282.
(18) Dikanov, S. A.; Samoilova, R. I.; Kolling, D. R. J.; Holland, J. T.; Crofts, A. R. *J. Biol. Chem.* **2004**, *279*, 15814–15823.
(19) Yap, L. L.; Samoilova, R. I.; Gennis, R. B.; Dikanov, S. A. *J. Biol. Chem.* **2006**, *281*, 16879–16887.
(20) Lin, T.-J.; O'Malley, P. J. *J. Mol. Struct.: THEOCHEM* **2008**, *870*, 31–35.
(21) Martin, E.; Samoilova, R. I.; Narasimhulu, K. V.; Wraight, C. A.; Dikanov, S. A. *J. Am. Chem. Soc.* **2010**, *132*, 11671–11677.
(22) Vreven, T.; Byun, K. S.; Komaromi, I.; Dapprich, S.; Montgomery, J. A.; Morokuma, K.; Frisch, M. J. *J. Chem. Theor. Comput.* **2006**, *2*, 815–826.
(23) Frisch, M. J. et al. *Gaussian 03, Revision D.01*; Gaussian, Inc.: Pittsburgh PA, 2003.
(24) Schweiger, A., Jeschke, G. *Principles of Pulse Electron Paramagnetic Resonance*; Oxford University Press: Oxford, 2001; Chapters 10 and 11.
(25) Dikanov, S. A. In *New Advances in Analytical Chemistry*; Atta-ur-Rahman, Ed.; Gordon and Breach: Amsterdam, 2000; pp 523−568.
(26) Van Doorslaer, S.; Vinck, E. *Phys. Chem. Chem. Phys.* **2007**, *9*, 4620–4638.
(27) Dikanov, S. A.; Bowman, M. K. *J. Magn. Reson. Ser. A* **1995**, *116*, 125–128.
(28) Dikanov, S. A.; Tyryshkin, A. M.; Bowman, M. K. *J. Magn. Reson.* **2000**, *144*, 228–242.
(29) Gemperle, C.; Aebli, G.; Schweiger, A.; Ernst, R. R. *J. Magn. Reson.* **1990**, *88*, 241–256.
(30) Stoll, S.; Calle, C.; Mitrikas, G.; Schweiger, A. *J. Magn. Reson.* **2005**, *177*, 93–101.
(31) Kolling, D. R. J.; Samoilova, R. I.; Shubin, A. A.; Crofts, A. R.; Dikanov, S. A. *J. Phys. Chem. A* **2009**, *113*, 653–667.
(32) Reijerse, E. J.; Dikanov, S. A. *J. Chem. Phys.* **1991**, *95*, 836–845.
(33) O'Malley, P. J.; Babcock, G. T. *J. Am. Chem. Soc.* **1986**, *108*, 3995–4001.
(34) MacMillan, F.; Lendzian, F.; Lubitz, W. *Magn. Reson. Chem.* **1995**, *33*, 581–593.
(35) Flores, M.; Isaacson, R. A.; Calvo, R.; Feher, G.; Lubitz, W. *Chem. Phys.* **2003**, *294*, 401–413.
(36) O'Malley, P. J. *Chem. Phys. Lett.* **1998**, *291*, 367–374.
(37) O'Malley, P. J. *Chem. Phys. Lett.* **1996**, *262*, 797–800.
(38) Rohrer, M.; MacMillan, F.; Prisner, T. F.; Gardiner, A. T.; Möbius, K.; Lubitz, W. *J. Phys. Chem. B* **1998**, *102*, 4648–4657.
(39) Schnegg, A.; Dubinskii, A. A.; Fuchs, M. R.; Grishin, Yu.A.; Kirilina, E. P.; Lubitz, W.; Plato, M.; Savitsky, A.; Möbius, K. *Appl. Magn. Reson.* **2007**, *31*, 59–98.
(40) Wraight, C. A.; Vakkasoglu, A. S.; Poluektov, Y.; Mattis, A.; Takahashi, E.; Nihan, D.; Lipshutz, B. H. *Biochim. Biophys. Acta* **2008**, *1777*, 631–636.
(41) Deligiannakis, Y.; Hanley, J.; Rutherford, A. W. *J. Am. Chem. Soc.* **1999**, *121*, 7653–7664.
(42) Humphrey, W.; Dalke, A.; Schulten, K. *J. Mol. Graphics* **1996**, *14*, 33–38.